Design of broad and large physical responses from atomistic simulations

Alireza Akbarzadeh, Yousra Nahas, Sergei Prokhorenko, and Laurent Bellaiche
Physics Department and Institute for Nanoscience and Engineering, University of Arkansas, Fayetteville, Arkansas 72701, USA

(Received 4 August 2020; accepted 9 September 2020; published 2 October 2020)

Using an effective Hamiltonian scheme within classical Monte Carlo simulations, we numerically investigate the effect of epitaxial strain on various physical quantities of the promising lead-free $(1-x)$Ba$(Zr_{0.2}Ti_{0.8})O_3$–$x(Ba_{0.7}Ca_{0.3})TiO_3$ solid solutions for different compositions. It is found that some combinations of strain and concentration lead to physical responses that are not only broad with temperature around 300 K but also large, including dielectric and piezoelectric coefficients. The origins of these useful and striking features are revealed.

DOI: 10.1103/PhysRevB.102.134202

I. INTRODUCTION

Ever since the increase of concerns about the impacts of hazardous lead-based materials on the environment, scientists have searched for environmentally friendly new materials. Among these materials are ones with large physical electromechanical responses, i.e., lead-free piezoelectrics [1–11]. This goal has led to the design or discovery of a few of such compounds, for instance some $BaTiO_3$ based systems. However, the piezoelectric responses of lead-free ceramics are usually smaller than that of Pb-based systems, such as Pb(Zr,Ti)O_3 (PZT), although a few Pb-free systems now show significant electromechanical response [3,11].

In the last decade, the discovery of $(1-x)$Ba$(Zr_{0.2}Ti_{0.8})O_3$–$x(Ba_{0.7}Ca_{0.3})TiO_3$ (to be denoted by BCTZ $-$ x in the following) with a relatively large piezoelectric response ($d_{33} \simeq$ 620 pC/N) [3], has sparked promise among research groups across the globe. In this system, Liu *et al.* followed the idea of playing with the composition to generate a morphotropic phase boundary (MPB), by placing different ferroelectric phases in close proximities to one another, and as a result paved the way for acquiring large piezoelectric and dielectric responses [3]. However, these physical responses in lead-free ceramics, like those in many other compounds, are only large for temperatures located very near a phase transition. This can limit technological applications that require large responses over a *broad* range of temperature to, e.g., accommodate temperature changes the devices can be subject to in their environment.

Here, we wish to address the following technologically and fundamentally important questions: (a) Is it possible to design a material, including a lead-free one, that can have large and broad physical responses, including dielectric and piezoelectric coefficients, especially around room temperature? (b) What are the microscopic local features responsible for these hypothetical enhanced physical responses?

Our approach consists of tuning epitaxial strains in epitaxial thin films made of BCTZ $-$ x, in order to induce several phases, including ferroelectric ones, energetically close to each other over a rather large temperature range. Note that thin films made of BCZT $-$ x have been successfully grown [12,13]. Practically, our atomistic simulations on BCTZ $-$ x (with $x = 0.15, 0.5, 0.845, 0.95$) films predict not only a large and broad dielectric response for $x = 0.845$ (0.5), but also a large and broad piezoelectric response over approximately 60 (30) K. Our microscopical analysis further reveals that these useful responses are associated with small sized and randomly scattered orthorhombic clusters of local dipoles embedded in the ferroelectric phase.

II. METHODOLOGY

Recently, we developed an effective Hamiltonian (H_{eff}) for $(1-x)$Ba$(Zr_{0.2}Ti_{0.8})O_3$–$x(Ba_{0.7}Ca_{0.3})TiO_3$ solid solutions [10,14], from first-principles calculations within the virtual crystal approximation (VCA) [15,16]. Specifically, in the VCA, the $\langle A\rangle\langle B\rangle O_3$ perovskite system is such that the fictional $\langle A\rangle$ atom is a compositional average of Ba and Ca potentials (with, e.g., 88% and 12% contributions, respectively, for BCTZ $-$ 0.4) while the average $\langle B\rangle$ atom is built from a mixing of the Zr and Ti potentials (with, e.g., 12% and 88% contributions, respectively, for BCTZ $-$ 0.4) [10,14].

Using this H_{eff}, we previously accurately reproduced the temperature-vs-composition diagram for BCTZ $-$ x for the entire compositional space, i.e., for $0 \leqslant x \leqslant 1$, and shed light on the origins of the giant piezoelectric response of BCTZ $-$ 0.5 and 0.4 [10]. In particular and in agreement with experiments [3–6], the simulated phase diagram confirmed the existence of a phase convergence region near room temperature, which automatically results in large dielectric and piezoelectric responses in BCTZ $-$ 0.5 and 0.4 compounds near 300 K [12]. We also further predicted a quantum-induced orthorhombic ground state for some narrow compositional range in BCTZ $-$ x, which was then experimentally confirmed [14,17,18].

Here, we use such H_{eff} to study the effect of epitaxial strain on physical responses of (001) epitaxial films made of BCTZ $-$ x. Technically, we follow the formulations of Ref. [19], in which the degrees of freedom of this H_{eff} are the local soft mode $\mathbf{u}_i$ of each five-atom unit

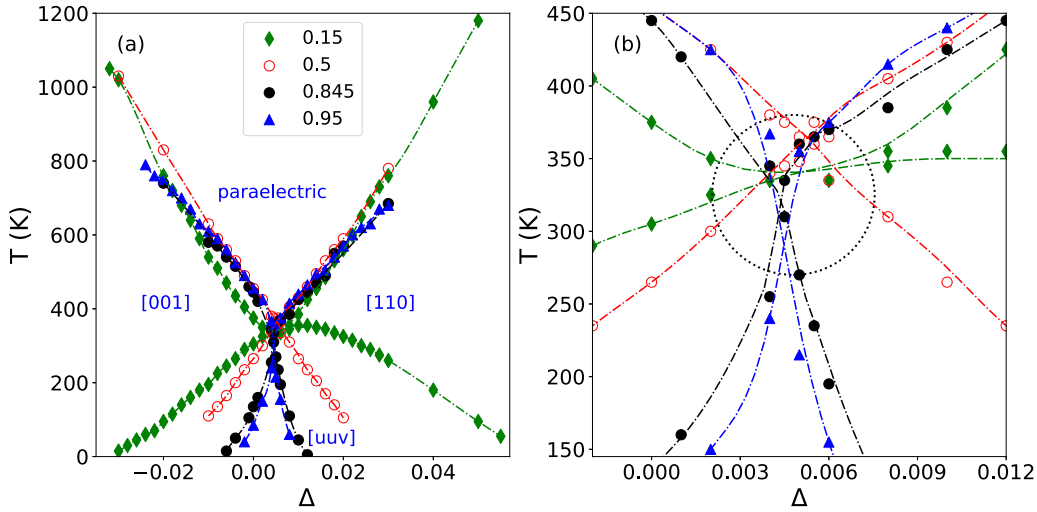

FIG. 1. (a) Predicted Pertsev phase diagram, i.e., temperature vs misfit strains in BCTZ $-x$ (with $x = 0.15$, 0.5, 0.845, and 0.95). Dotted lines are guides to the eye. (b) Zoom-in of panel (a) over a narrow temperature and strain window, with the dashed circle showing the region where all four phases coexist for different compositions. Error bars on calculated transition temperature are approximately ± 7 K.

cell (which is proportional to the electric dipole moment of cell i), inhomogeneous-strain-related dimensionless displacements $\{\mathbf{v}_i\}$, and the homogeneous strain tensor η. The latter is relevant to mechanical boundary conditions since epitaxial (001) films are associated with the freezing of some components of the homogeneous strain, namely (in Voigt notation) $\eta_6 = 0$ and $\eta_1 = \eta_2 = \Delta$, where $\Delta = \frac{a_{\text{sub}} - a_0}{a_0}$ is the misfit strain with its value forcing the film to adopt the a_{sub} in-plane lattice constant of the substrate [20–22], and with a_0 being the composition-dependent lattice constant of cubic bulk BCTZ $-x$ interpolated to 0K.

In the present study, we use $12 \times 12 \times 12$ supercells (that are periodic along any $\langle 001 \rangle$ direction) and vary Δ, to mimic the growth on different substrates imposing epitaxial strains. Generally, we run 10^7 classical Monte Carlo (CMC) sweeps to obtain transition temperatures. We used the first half of these sweeps for thermalization and then the second half to calculate statistical averages of various physical properties.

III. RESULTS AND DISCUSSIONS

Figure 1(a) shows the so-called Pertsev phase diagram [21] of the predicted transition temperature vs epitaxial strain for different compositions in BCTZ $-x$, namely for $x = 0.15$, 0.5, 0.845, and 0.95. Transition temperatures are derived using information provided by the supercell average of the local modes vs temperature graphs for each selected strain and composition (not shown here).

Four phases are observed: a paraelectric phase at high temperatures, a tetragonal phase with a polarization pointing along the [001] pseudocubic direction for some (mostly compressive) strains, an orthorhombic phase with a polarization lying along the [110] pseudocubic direction for some tensile strains, and finally a monoclinic phase with a polarization being oriented along $[uuv]$ directions for some strains basically centered around the zero value. This latter phase exhibits a rotation of its polarization between [001] and [110] directions when going from the border with the tetragonal phase to the border with the orthorhombic state. All the aforementioned four phases are known to occur in other epitaxial ferroelectric thin films (see, e.g., Refs. [23–26] and references therein).

Our simulations show that, as the Ca composition in BCTZ $-x$ increases (i.e., when x is enhanced), the strain range of stability of the monoclinic phase becomes narrower. For instance, for our four investigated compositions, the narrowest monoclinic phase corresponds to $x = 0.95$ and spans from -0.002 compressive strain to $+0.008$ tensile strain, at the lowest temperatures. This is to be compared with the widest monoclinic state occurring for $x = 0.15$ from -0.03 to $+0.055$ strains. We numerically found that the width of the strain stability region of the monoclinic state in the films is directly correlated with the stability of the rhombohedral $R3m$ phase in the bulk: the deeper the energy is of this rhombohedral state in the bulk case (as in $x = 0.15$ for which the ground state is rhombohedral, in contrast with $x = 0.95$ for which the predicted ground state is tetragonal), the wider is the monoclinic strain region in the corresponding (001) film.

Furthermore, Fig. 1(b) is a zoom-in of the transition temperatures vs strains in BCTZ $-x$ for a specific window of strains. It shows that all four aforementioned phases can be found within a temperature window near room temperature. For instance, in BCTZ $-$ 0.845 (respectively, 0.5) subject to a strain of $+0.0045$ ($+0.005$), the evolution of the supercell average of the local modes vs temperature indicates (data not shown here) that a paraelectric-to-ferroelectric orthorhombic transition occurs around $\simeq$ 335 K (a paraelectric-to-ferroelectric tetragonal around $\simeq$ 365 K), followed by a transition to a ferroelectric monoclinic phase around 310 K ($\simeq$ 348 K). The simulations also predict that, in BCTZ $-$ 0.95 and for a strain of $+0.004$, a transition from paraelectric-to-ferroelectric tetragonal happens around 367 K followed by a transition to the ferroelectric monoclinic phase around 245 K. In the case of $x = 0.15$, at a strain of $+0.002$ (respectively, $+0.008$), a transition from paraelectric-to-ferroelectric tetragonal (respectively, orthorhombic) occurs at $\simeq$ 350 K (respectively, $\simeq$ 355 K) and then the system becomes monoclinic

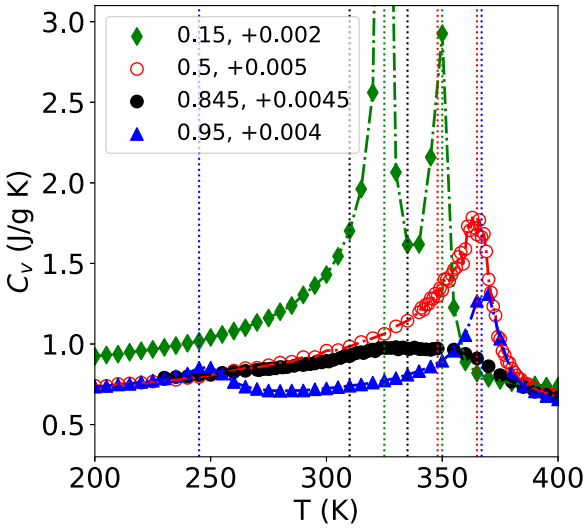

FIG. 2. Specific heat as a function of temperature in BCTZ − x (with $x = 0.15$, 0.5, 0.845, and 0.95) under specific epitaxial strains. Vertical dotted lines show the transition temperatures (recalling that error bars on calculated transition temperatures are approximately ±7 K).

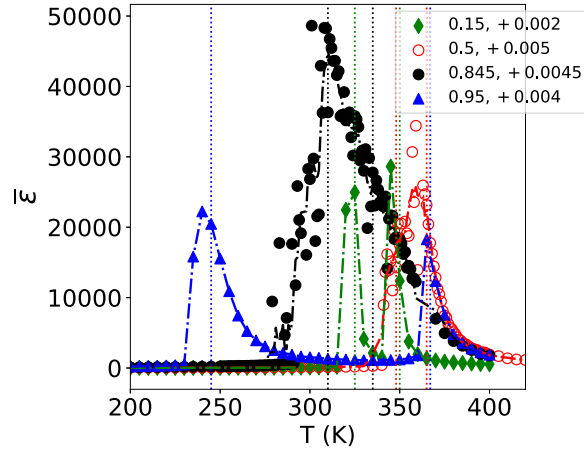

FIG. 3. Average dielectric response in epitaxial BCTZ − x ($x =$ 0.15, 0.5, 0.845, and 0.95) vs temperature for some selected strains. Vertical dotted lines show the transition temperatures (recalling that error bars on calculated transition temperatures are approximately ±7 K).

at ≃ 325 K (respectively, ≃ 345 K). Note that the average error bar of all these transition temperatures can be estimated to be about ±7 K.

Note that the aforementioned transitions for $x = 0.95$ at a strain of +0.004 and for $x = 0.15$ at a strain of +0.002 can also be clearly identified by the two peaks of the specific heat, as calculated using the fluctuations theorem [27] and displayed in Fig. 2 for these two combinations of composition and strain. Interestingly, this latter figure also reveals that, for BCTZ − 0.5 under a strain of +0.005, the specific heat exhibits a peak at the paraelectric-to-tetragonal transition of ≃ 365 K while it is difficult to observe a second peak at the tetragonal-to-monoclinic transition of ≃ 348 K, likely because this hypothetical second peak is "embedded" in the shoulder of the peak associated with the paraelectric-to-ferroelectric transition occurring only ≃ 20 K higher.

Another striking feature of Fig. 2 is the broad specific heat for $x = 0.845$ at a strain of +0.0045, with this physical quantity being basically temperature independent in the region delimiting the paraelectric-to-orthorhombic and orthorhombic-to-monoclinic transitions. Figure 2 therefore shows that varying the composition and strain in epitaxial (001) BCTZ − x films can dramatically modify the values but also shape of physical responses, in general, and make some properties broad with temperature in particular, owing to the proximity of several phases.

This fact motivated us to calculate the dielectric response for the same four combinations of composition and strain as in Fig. 2, using the correlation function method of Ref. [28]. More precisely, we computed one third of the trace of the dielectric response tensor, and report it as a function of temperature in Fig. 3 for each of these combinations. The calculations reveal the possibility of generating large dielectric response over a wide temperature window in epitaxial BCTZ − x films for some specific strains. For instance, our CMC simulations predict that the dielectric response of the composition $x = 0.845$ at $\Delta = +0.0045$ reaches values larger than 10 000 over the ≃ 60 K temperature window varying from 290 K to 350 K. Such large and broad response can be understood by realizing that the results shown in Fig. 1(b) indicate that the paraelectric and ferroelectric tetragonal, monoclinic, and orthorhombic states are all energetically close to each other for this composition and strain for that temperature range as evidenced by (i) the aforementioned paraelectric-to-orthorhombic and orthorhombic-to-monoclinic transition temperatures of ≃ 335 and ≃ 310 K, respectively, and (ii) the narrow strain range for which the monoclinic state is the equilibrium state around ≃ 310 K.

Note also that Fig. 3 further shows that the composition $x = 0.5$ at $\eta_1 = \eta_2 = \Delta = +0.0050$ has a rather broad and large dielectric response but at higher temperatures located around 365 K (which may be useful for applications requiring optimization of responses above room temperature) because of (iii) the occurrence of a paraelectric-to-ferroelectric tetragonal transition at 365 K and a ferroelectric-tetragonal-to-ferroelectric-monoclinic phase transition at around 348 K, and (iv) a narrow strain range for the monoclinic phase at $T = 348$ K [see Fig. 1(b)].

In contrast, the compositions $x = 0.95$ at $\Delta = +0.0040$ and $x = 0.15$ at $\Delta = +0.0020$ show large but rather narrow dielectric responses, because the two successive transitions in the case of $x = 0.95$ occur at 367 and 245 K (i.e., they are far away) while, in the case of $x = 0.15$, the strain range of stability of the monoclinic state is rather large around 337 K (see Fig. 1). The latter implies that the other phases have much higher free energy than the monoclinic state around 337 K in that case (even if the two phase transitions of ≃ 350 and ≃ 325 K are distinct by only about 25 K). Consequently, for the composition $x = 0.15$ and a strain of +0.002, the dielectric response at about 337 K is rather small.

Let us thus now concentrate on the two promising compositions at their selected specific strains, which are BCTZ − 0.845 at $\Delta = +0.0045$ and BCTZ − 0.5 at $\Delta = +0.0050$,

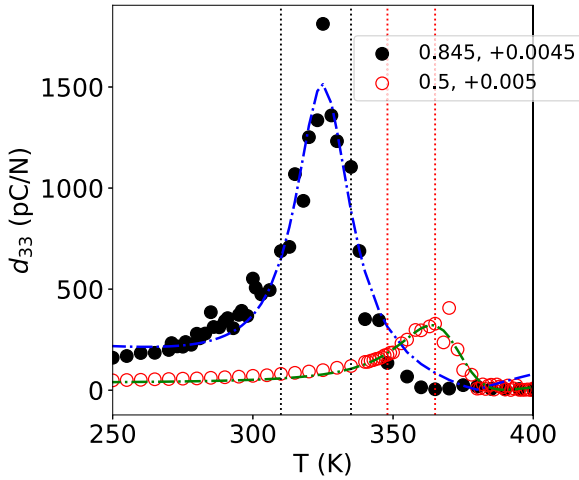

FIG. 4. Calculated d_{33} piezoelectric coefficients as a function of temperature in epitaxial BCTZ $-x$ (with $x = 0.5$ and 0.845) for selected misfit strains. Blue and green dashed-dotted lines are guides for the eye. Vertical dotted lines show the transition temperatures (recalling that error bars on calculated transition temperatures are approximately ± 7 K).

and compute their electromechanical responses. Figure 4 shows the absolute value of the d_{33} piezoelectric coefficient (in the orthonormal basis formed by the [100], [010], and [001] pseudocubic directions) for these two cases. Here, we used the correlation function approach of Ref. [28] to calculate d_{33}. A very prominent feature in the simulations indicates that d_{33} is rather broad and large with temperature for both cases. In particular, our calculations yield a d_{33} that ranges between $\simeq 135$ and >1400 pC/N ($\simeq 100$ and $\simeq 400$ pC/N) when temperature varies from 290 to 350 K (340 to 375 K) in the case of $x = 0.845$ (0.5).

Interestingly, we also noticed that d_{33} has a maximum located at $T_{\max} \simeq 325$ K, that is in between, rather than at, the transition temperatures (dotted vertical lines in Fig. 4) for $x = 0.845$ (note that $T_{\max}$ is the temperature at which the d_{33} piezoelectric coefficient is maximum in our notations). While we cannot exclude that this striking feature is due to large error bars inherent to the large fluctuations obtained during the simulations [29], we rather believe that it originates from the aforementioned close proximity of several phases for this particular combination of composition and strain.

IV. CLUSTER ANALYSIS

In order to gain a deeper insight into the origins of the large piezoelectric response, we further decided to investigate some local structures associated with clusters of dipoles. More precisely, a modified Hoshen-Kopelman algorithm [30,31] is used to perform such analysis in the case of $x = 0.5$ at a strain of $+0.0050$, and for the composition of 0.845 at a strain of $+0.0045$. Specifically, we looked at three types of clusters, namely tetragonal (T), orthorhombic (O), and rhombohedral (R) that correspond to dipoles belonging to a certain region of space inside which dipoles are parallel to each other and are close to $\langle 001 \rangle$, $\langle 110 \rangle$, or $\langle 111 \rangle$ pseudocubic directions, respectively. The threshold for classifying these clusters is that

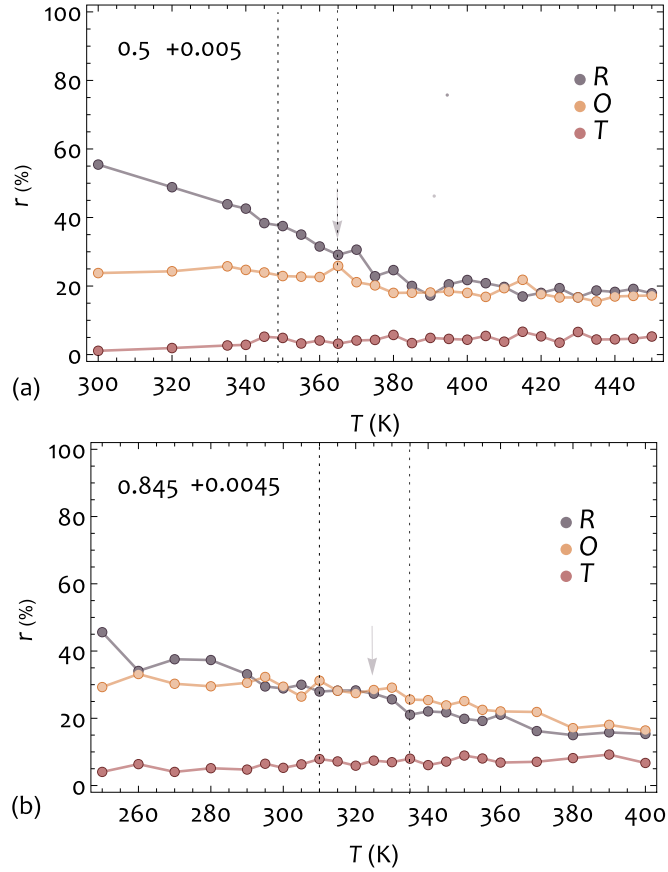

FIG. 5. (a) and (b) Relative volume occupancy of the different R, O, and T types of cluster vs temperature in BCTZ $-x$, with $x = 0.5$ and 0.845 and for some selected strains, respectively. Vertical dotted lines show the transition temperatures (recalling that error bars on calculated transition temperatures are approximately ± 7 K), while the arrows point to $T_{\max}$, that is, the temperature at which d_{33} is maximum in Fig. 4.

the projection of a dipole on the aforementioned directions should be at least 90% of the magnitude of that dipole so as to be considered belonging to the corresponding clusters.

The results are presented in Figs. 5(a) and 5(b), in which the panels show the temperature evolution of the *relative* volume occupation of each type of clusters; that is, the ratio between the number of sites occupied by all clusters of one type over the whole number of sites in the supercell.

Panel (a) of Fig. 5 shows that, in case of $x = 0.5$ and under strain of $+0.0050$, the R and O clusters have a similar ratio close to 20% for temperatures greater than 365 K, while the percent of T clusters is very small. Interestingly, a further analysis (not shown here) indicates that, at 365 K, summing the dipoles belonging to these microscopic O and R clusters results in a macroscopic dipole lying along a tetragonal $\langle 001 \rangle$ direction, as consistent with the evolution of the supercell average of the local modes versus temperature. In other words, the microscopic and tetragonal macroscopic structures are very different here. Moreover, for temperatures lower than 360 K, the volume occupancy of the R clusters gradually grows faster than the O clusters, and, e.g., occupies more than 55% of the supercell volume at $\simeq 300$ K, while that of the O clusters almost remains the same around 25% for all

these temperatures. Note that, consistently with Fig. 1, adding the dipoles of such clusters at around $\simeq 348$ K basically yields a monoclinic phase. In other words, local and global structures differ once again greatly even in the monoclinic phase for $x = 0.5$ and under strain of $+0.0050$ at these lower temperatures.

Regarding the case of $x = 0.845$ at $+0.0045$ tensile strain, panel (b) of Fig. 5 indicates that the R and O clusters gradually increase almost at same rate when decreasing the temperature from 400 to 250 K. Meanwhile, the volume occupancy of the T clusters is low here too at all temperatures. Once again, we find that the microscopic picture made of various clusters with different orientations for their dipoles contrasts with the macroscopic structure since this combination of composition and strain yields global macroscopic ferroelectric orthorhombic and monoclinic states, depending on the temperature below 335 K.

We now focus on the $T_{\max}$ temperature for which the d_{33} piezoelectric response is a maximum, that is $\simeq 365$ K for $x = 0.5$ at $+0.0050$ and $\simeq 325$ K in case of $x = 0.845$ at $+0.0045$. In Figs. 6(a)–6(c) we plotted the probability density function f_s (its integral over the entire space is equal to 1) of cluster sizes at $T_{\max}$ and for the two selected compositions and strains. One can realize from Fig. 6 that, for all types of clusters, f_s in $x = 0.5$ and 0.845 bears similarity (especially for the R clusters) except that $x = 0.845$ has an enhanced distribution of T and O clusters at small size. Such enhancement is characteristic of a more "fragmented" local structure, that is a more disordered and more inhomogeneous local structure. Due to the fact that Figs. 5(a) and 5(b) clearly demonstrate that there are many more O clusters than T clusters, one can then conclude that the existence of many small O clusters plays an important role in the giant electromechanical response and makes it possible for the composition 0.845 at $+0.0045$ tensile strain to have remarkably large $d_{33} \simeq 1400$ pC/N at 330 K (Fig. 4). Interestingly, such enhancement of piezoelectricity due to fragmented local structures has been previously noted in *bulk* BCTZ $- 0.5$ [10]. Such facts, as well as the finding of Ref. [32], therefore emphasize that having local structural inhomogeneity is a key ingredient to obtain large electromechanical response, which is presently and originally done by playing with composition and strain here.

V. CONCLUSIONS

In summary, effects of epitaxial strains on physical responses in BCTZ $- x$ have been probed using first-principle-based effective Hamiltonian simulations. Specifically, we constructed a temperature-vs-misfit strain diagram and calculated specific heat, dielectric response, and piezoelectric coefficient d_{33} for compositions $x = 0.15, 0.5, 0.845$, and 0.95 at selected strains. The results especially yield very promising broad and large physical responses in case of $x = 0.845$ around room temperature. Such useful features are found to originate from the active role of strain (1) to bring different phases energetically close to each other within a large enough temperature window involving 300 K; and (2) to induce inhomogeneity in local structures. We hope that these striking results, and their associated guidelines, will encourage researchers to design novel multifunctional materials, including lead-free ones, having broad and large responses.

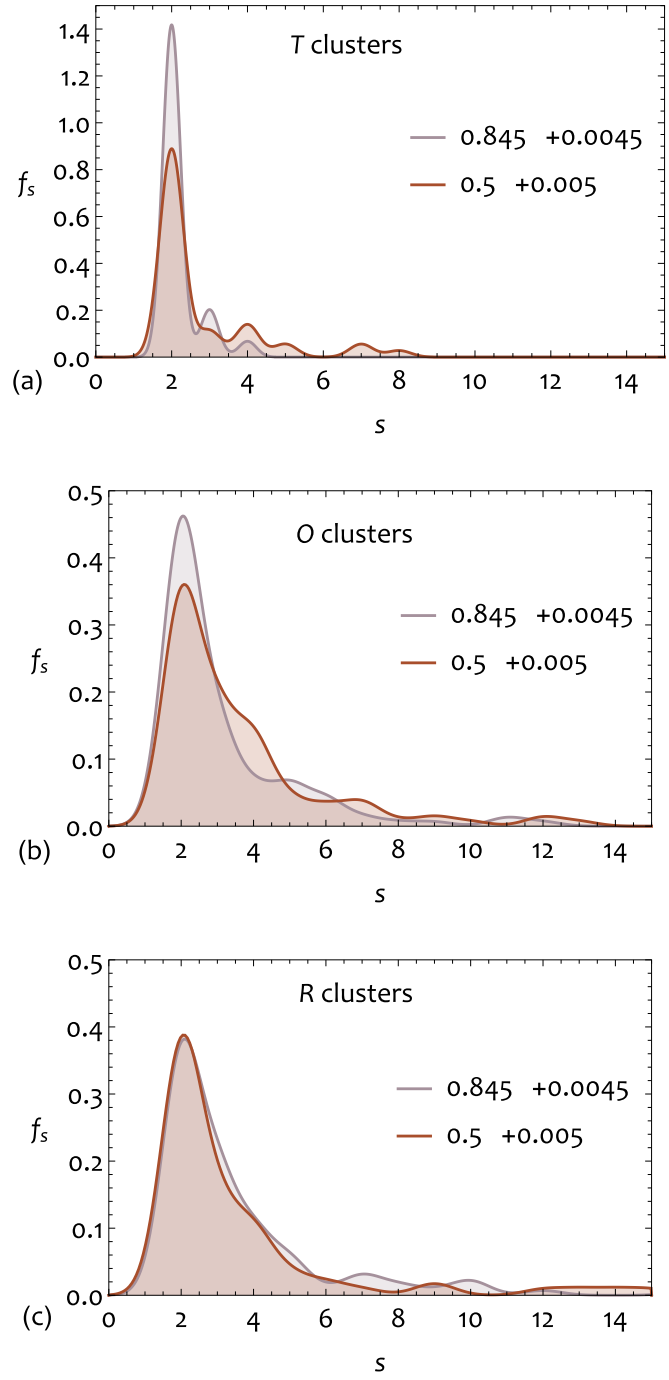

FIG. 6. (a)–(c) probability density f_s for different size and type of clusters, i.e., T, O, and R, in BCTZ $- 0.5$ at$+0.005$ strain and a temperature of 365 K, as well as in BCTZ $- 0.845$ at $+0.0045$ strain and a temperature of 325 K.

ACKNOWLEDGMENTS

A.A., S.P. and L.B. acknowledge support via DARPA Grant No. HR0011-15-2-0038 (MATRIX program). Y.N. and L.B. acknowledge support via DARPA Grant No. HR0011727183-D18AP00010 (TEE program). Y.N., S.P. and L.B. also thank the Vannevar Bush Faculty Fellowship (VBFF) Grant No. N00014-20-1-2834 from the Department of Defense.

[1] European Commission, Directive 2002/95/EC of the European Parliament and of the Council of 27 January 2003 on the restriction of the use of certain hazardous substances in electrical and electronic equipment, Off. J. Eur. Union **L37**, 19 (2003).

[2] European Commission, Directive 2011/65/EU of the European Parliament and of the Council of 8 June 2011 on the restriction of the use of certain hazardous substances in electrical and electronic equipment, Off. J. Eur. Union **L174**, 88 (2011).

[3] W. Liu and X. Ren, Phys. Rev. Lett. **103**, 257602 (2009).

[4] D. S. Keeble, F. Benabdallah, P. A. Thomas, M. Maglione, and J. Kreisel, Appl. Phys. Lett. **102**, 092903 (2013).

[5] G. Tutuncu, B. Li, K. Bowman, and J. L. Jones, J. Appl. Phys. **115**, 144104 (2014).

[6] M. Acosta, N. Khakpash, T. Someya, N. Novak, W. Jo, H. Nagata, G. A. Rossetti Jr., and J. Rödel, Phys. Rev. B **91**, 104108 (2015).

[7] A. Piorra, A. Petraru, H. Kohlstedt, M. Wuttig, and E. Quandt, J. Appl. Phys. **109**, 104101 (2011).

[8] K. Brajesh, M. Abebe, and R. Ranjan, Phys. Rev. B **94**, 104108 (2016).

[9] K Brajesh, K. Tanwar, M. Abebe, and R. Ranjan, Phys. Rev. B **92**, 224112 (2015).

[10] Y. Nahas, A. R. Akbarzadeh, S. Prokhorenko, S. Prosandeev, R. Water, I. Kornev, J. Íñiguez, and L. Bellaiche, Nat. Commun. **8**, 15944 (2017).

[11] Y. Saito, H. Takao, T. Tani, T. Nonoyama, K. Takatori, T. Homma, T. Nagaya, and M. Nakamura, Nature (London) **432**, 84 (2004).

[12] N. D. Scarisoreanu, F. Craciun, A. Moldovan, V. Ion, R. Birjega, C. Ghica, R. F. Negrea, and M. Dinescu, Appl. Mater. Interfaces **7**, 23984 (2015).

[13] V. Ion, F. Craciun, N. D. carisoreanu, A. Moldovan, A. Andrei, R. Birjega, C. Ghica, D. F. Pietrantonio, D. Cannata, M. Benetti, and M. Dinescu, Sci. Rep. **8**, 2056 (2018).

[14] A. R. Akbarzadeh, K. Brajesh, Y. Nahas, N. Kumar, S. Prokhorenko, D. Swain, S. Prosandeev, R. Walter, I. Kornev, J. Íñiguez, B. Dkhil, R. Ranjan, and L. Bellaiche, Phys. Rev. B **98**, 104101 (2018).

[15] J. A. Van Vechten, Phys. Rev. **182**, 891 (1969).

[16] L. Bellaiche and D. Vanderbilt, Phys. Rev. B **61**, 7877 (2000).

[17] L. Bellaiche, A. Garcia, and D. Vanderbilt, Ferroelectrics **266**, 41 (2002).

[18] Note that Nahas *et al.* [10] reproduced very well the phase diagram of (Ba, Ca)(Zr, Ti)O_3 systems by simply using the VCA approach. They also reproduced and explained, once again, within the VCA approach, the large piezoelectricity observed for some compositions via the appearance of different local clusters, as a result of the existence of several phases that are energetically close to each other. In other words, it appears that VCA can mimic rather well (Ba, Ca)(Zr, Ti)O3 systems, likely because Ba and Ca ions belong to the same column of the periodic table, as Ti and Zr ions do. Consequently, random fields arising from true alloying (generating a local change in composition) are probably small, similarly to what was found in Ref. [17], where the random fields arising from Ti/Zr substitutions in $Pb(Zr_{1-x}Ti_x)O_3$ systems were shown to be small.

[19] W. Zhong, D. Vanderbilt, and K. M. Rabe, Phys. Rev. Lett. **73**, 1861 (1994); Phys. Rev. B **52**, 6301 (1995).

[20] I. Kornev, H. Fu, and L. Bellaiche, Phys. Rev. Lett. **93**, 196104 (2004).

[21] N. A. Pertsev, V. G. Kukhar, H. Kohlstedt, and R. Waser, Phys. Rev. B **67**, 054107 (2003).

[22] O. Diéguez, S. Tinte, A. Antons, C. Bungaro, J. B. Neaton, K. M. Rabe, and D. Vanderbilt, Phys. Rev. B **69**, 212101 (2004).

[23] A. R. Akbarzadeh, L. Bellaiche, J. Íñiguez, and D. Vanderbilt, Appl. Phys. Lett. **90**, 242918 (2007).

[24] B.-K. Lai, I. A. Kornev, L. Bellaiche, and G. Salamo, Appl. Phys. Lett. **86**, 132904 (2005).

[25] R. Aso, D. Kan, Y. Shimakawa, and H. Kurata, Sci. Rep. **3**, 2214 (2013).

[26] C. Ghica, R. F. Negrea, L. C. Nistor, C. F. Chirila, and L. Pintilie, J. Appl. Phys. **116**, 023516 (2014).

[27] S. Bin-Omran, I. A. Kornev, and L. Bellaiche, Phys. Rev. B **93**, 014104 (2016).

[28] A. Garcia and D. Vanderbilt, in *First-Principles Calculations for Ferroelectrics: Fifth Williamsburg Workshop*, edited by R. E. Cohen (AIP, New York, 1998), pp. 53–60.

[29] We initially ran 10^7 CMC sweeps to calculate physical responses. However, we noticed very large fluctuations in local modes near and in between transition temperatures and thus large fluctuations in the piezoelectric coefficient d_{33}. Thus, starting from the last configurations of local dipoles and strains, we ran multiple CMC simulations with 10^6 sweeps each time using the previous configurations for up to 13 times. The results represented in Fig. 4 for temperatures near and in between phase transitions are the average of those individual runs, in order to get a smooth behavior.

[30] J. Hoshen and R. Kopelman, Phys. Rev. B **14**, 3438 (1976).

[31] Y. Nahas, Gauge theory for relaxor ferroelectrics. Ph.D. thesis, Ecole Centrale Paris, 2013.

[32] F. Li, M. J. Cabral, B. Xu, Z. Cheng, E. C. Dickey, J. M. LeBeau, J. Wang, J. Luo, S. Taylor, W. Hackenberger, L. Bellaiche, Z. Xu, L. Chen, T. R, and S. Zhang, Science **364**, 264 (2019).